

Revisiting the orbital tracking problem

John T. Kent¹ and Shambo Bhattacharjee²
University of Leeds, Leeds, UK

Weston R. Faber³
L3Harris, Applied Defense Solutions, Colorado Springs, CO, USA

Islam I. Hussein⁴
L3Harris, Applied Defense Solutions, Herndon, VA, USA

Consider a space object in an orbit about the earth. An uncertain initial state can be represented as a point cloud which can be propagated to later times by the laws of Newtonian motion. If the state of the object is represented in Cartesian earth centered inertial (Cartesian-ECI) coordinates, then even if initial uncertainty is Gaussian in this coordinate system, the distribution quickly becomes non-Gaussian as the propagation time increases. Similar problems arise in other standard fixed coordinate systems in astrodynamics, e.g. Keplerian and to some extent equinoctial. To address these problems, a local “Adapted STructural (AST)” coordinate system has been developed in which uncertainty is represented in terms of deviations from a “central state”. Given a sequence of angles-only measurements, the iterated nonlinear extended (IEKF) and unscented (IUKF) Kalman filters are often the most appropriate variants to use. In particular, they can be much more accurate than the more commonly used non-iterated versions, the extended (EKF) and unscented (UKF) Kalman filters, especially under high eccentricity. In addition, iterated Kalman filters can often be well-approximated by two new closed form filters, the observation-centered extended (OCEKF) and unscented (OCUKF) Kalman filters.

¹ Professor, Department of Statistics, j.t.kent@leeds.ac.uk.

² PhD student, Department of Statistics, mmsb@leeds.ac.uk.

³ Research Scientist, weston.faber@l3harris.com.

⁴ Senior R&D Scientist, islam.Hussein@l3harris.com.

I. Introduction

This paper revisits the filtering problem for an object in orbit about the earth. The aim is to give a *better solution* than earlier authors. Recall the orbital filtering problem is nonlinear: depending on the coordinate system, either the system equation or the observation equation (or both) is nonlinear, thus complicating the implementation of the propagation and/or update equations in the filter. The proposed solution uses a coordinate system in which the filtering problem almost reduces to a linear Gaussian system, so that a mild variant of the classic Kalman filter can be used. In particular, the update equations have a simple (nearly) closed form and are (nearly) optimal.

For simplicity in this paper, assume the following *idealized conditions*:

- (a) initial Gaussian uncertainty in Cartesian-ECI coordinates,
- (b) Keplerian dynamics for the evolution of the state of the object, and
- (c) a sequence of angles-only measurements made by an ideal observer at the center of the earth following a concentrated Fisher distribution on the unit sphere.

Attention is limited to idealized conditions in this paper so that the key features of our solution can be clearly understood. Assumption (a) is a common assumption in this area. The extension of assumptions (b) and (c) to more realistic conditions (e.g. to accommodate the perturbation effects of the earth's gravity and to locate observers on the surface of the earth) will be dealt with elsewhere.

The essence of the proposed procedure can be summarized as follows:

- (a) Represent the uncertainty in a new set of coordinates which are called AST coordinates. These coordinates are essentially a local version of equinoctial coordinates with some small modifications. In these coordinates the system equation is *exactly linear*.
- (b) Given an observation, carry out the update step of the filter using the iterated unscented Kalman filter (IUKF) [1].

Orbital uncertainty propagation and orbital object tracking are a key themes in Space Situational Awareness (SSA) and a number of papers have been published in recent years to deal with the nonlinearity of the system equation when expressed in Cartesian-ECI coordinates. There are two basic strategies to deal with nonlinearity: (i) transform the coordinate system to remove the nonlinearity, or (ii) develop sophisticated methods to accommodate it. As an example of the former approach, Junkins, Akella, and Alfriend [2] showed using point clouds that Gaussianity is approximately preserved under propagation in equinoctial coordinates in many circumstances. The current paper can be viewed as an extension of that point of view.

On the other hand, many other papers have taken the second approach. For example, Park and Scheeres [3] used a mixture (hybrid approach) of a simplified dynamic system (SDS) model and the state transition tensor (STT) model to propagate and model the uncertainty with higher order Taylor series terms [3–5]. Vittaldev, Russell and Linares [6] proposed a mixture of polynomial chaos expansion (PCE) and Gaussian Mixture Models (GMMs) based on Hermite polynomials. Several other papers [7, 8] also used the polynomial chaos model (PCM) and PCE for representing orbital uncertainty. Horwood and Poore [9] proposed a Gauss Von Mises (GVM) filter using second order trigonometric terms.

The paper is organized as follows. Section II briefly reviews some key ideas in orbital dynamics under Keplerian dynamics. Section III recalls some standard coordinate systems for the state vector and uses them to motivate the new AST coordinate system. The approximate linearity between Cartesian and AST coordinates at an initial time is explored in Sections IV and V. The filtering problem using AST coordinates is analyzed in Section VIII for a sequence of angles only measurements. It is demonstrated that a suitably formulated IUKF is nearly optimal under a wide range of conditions.

II. Review of Keplerian dynamics

A. Three angles in orbital dynamics

A small object orbiting the earth follows an exact elliptical orbit under Keplerian dynamics, with the center of the earth at one of the focal points of the ellipse. There are three angles of

mathematical interest in this setting to describe the angular position of the object along its orbit: the *eccentric anomaly* (E), the *mean anomaly* (M) and the *true anomaly* (T), where all three angles are measured from perigee. The true anomaly describes the actual angular position of the object, as measured from the center of the earth. The mean anomaly simplifies the mathematical development because it changes at a constant rate in time, and the eccentric anomaly is an intermediate angle of no direct interest. The relation between the angles is given as follows [10], where e is the ellipticity, $0 \leq e < 1$:

$$\tan \frac{1}{2}T = \sqrt{\frac{1+e}{1-e}} \tan \frac{1}{2}E,$$

$$M = E - e \sin E.$$

These mappings are bijective, so any one angle determines the other two. The calculations are all straightforward, except that a numerical iteration is needed to solve for E from M .

Initially all three angles are defined on the same interval $-\pi \leq E, M, T \leq \pi$. The angles agree at the midpoint and endpoints. That is, if $E = 0, \pi$ or $-\pi$, then M and T also equal to $0, \pi$ or $-\pi$, respectively. Further the identification between angles is symmetric about the origin. That is, if E corresponds to M and T , then $-E$ corresponds to $-M$ and $-T$. Finally, by periodic extension, the mapping between the three angles can be extended to any interval $-\pi + 2\pi k \leq E, M, T \leq \pi + 2\pi k$, $k \in \mathbb{Z}$.

The notation $E = F_{M\text{-to-}E}(M, e)$ is used to describe the transformation between M and E and similar notation for the transformations between other pairs of angles. The main transformations of interest are $F_{M\text{-to-}E}$ and $F_{E\text{-to-}M}$.

B. Equations of orbital motion

Consider the *state* of an object orbiting the earth. The state at time t can be described in Cartesian-ECI coordinates by three-dimensional position and velocity vectors $\mathbf{x}(t)$, $\dot{\mathbf{x}}(t)$, say. The state at any one time determines the state at all other times under Keplerian dynamics, and the object follows an elliptical orbit. Various features can be extracted from the state to help describe this elliptical orbit [10–13]. Here μ is the gravitational constant for the earth.

(a) In general, the term *basis* will be used in the paper as shorthand for a positively oriented

basis of three orthonormal vectors in \mathbb{R}^3 . In the current setting, a useful basis is the *RTN* (*radial-tangential-normal*) basis at an initial time $t = 0$, defined as follows:

$$\begin{aligned}\mathbf{u} &= \mathbf{u}^{\text{RTN}} \propto \mathbf{x}(0), \\ \mathbf{v} &= \mathbf{v}^{\text{RTN}} \propto \dot{\mathbf{x}}(0) - \{\dot{\mathbf{x}}(0)^T \mathbf{u}\} \mathbf{u}, \\ \mathbf{w} &= \mathbf{w}^{\text{RTN}} = \mathbf{u} \times \mathbf{v} \propto \mathbf{x}(0) \times \dot{\mathbf{x}}(0),\end{aligned}\tag{II.1}$$

so that \mathbf{u} points in the radial direction, \mathbf{v} points in the tangential direction (after orthogonalizing with respect to the radial direction) and \mathbf{w} is normal to the $\mathbf{u} - \mathbf{v}$ plane. This basis is positively oriented since $\det[\mathbf{u} \ \mathbf{v} \ \mathbf{w}] = +1$, not -1 .

(b) The *angular momentum vector* is given by $\mathbf{h} = \mathbf{x}(0) \times \dot{\mathbf{x}}(0) = h\mathbf{w}$, where magnitude $h = |\mathbf{h}|$ is called the *angular momentum*.

(c) The *ellipticity vector* is given by

$$\mathbf{e} = \frac{1}{\mu}(\dot{\mathbf{x}}(0) \times \mathbf{h}) - \mathbf{u}.$$

Its magnitude $e = |\mathbf{e}|$ is called the *ellipticity*, and for this paper it is assumed that $0 \leq e < 1$.

(d) The length of the *semi-major axis* of the ellipse (i.e., the arithmetic average of the radius of the orbit at perigee and apogee) is given by

$$a = \frac{h^2/\mu}{1 - e^2}.\tag{II.2}$$

(e) The *period* and the *mean motion* are

$$p = 2\pi\sqrt{a^3/\mu}, \quad n = 2\pi/p = \sqrt{\mu/a^3}.\tag{II.3}$$

(f) The *direction of perigee* is given by

$$\theta_p = \text{atan2}(\mathbf{e}^T \mathbf{v}, \mathbf{e}^T \mathbf{u})$$

and defines the angle in the $\mathbf{u} - \mathbf{v}$ plane at which the orbiting object is closest to the earth. Here atan2 is the two-argument arctan function found in many computing languages. For example, $\theta_p = 0$ points towards the positive \mathbf{u} axis and $\theta_p = \pi/2$ points towards the positive \mathbf{v} axis.

The ellipticity vector lies in the $\mathbf{u} - \mathbf{v}$ plane and can be written in the form

$$\mathbf{e} = f_1 \mathbf{u} + f_2 \mathbf{v},\tag{II.4}$$

where $f_1 = e \cos \theta_p$ and $f_2 = e \sin \theta_p$.

The Cartesian-ECI coordinates of the state can be computed from any 6 functionally independent features, such as the following:

$$\begin{aligned}
& \text{the } \mathbf{u}, \mathbf{v}, \mathbf{w} \text{ basis, (3 degrees of freedom)} \\
& \text{the ellipticity coordinates } f_1, f_2 \text{ (2 degrees of freedom)} \\
& \text{the mean motion } n \text{ (one degree of freedom).}
\end{aligned} \tag{II.5}$$

Note this information does not yet form a coordinate system because we have not yet given an explicit representation for the vectors $\mathbf{u}, \mathbf{v}, \mathbf{w}$.

The preceding information can be used to describe the evolution of an orbiting object in time under Keplerian dynamics. Note the basis $\mathbf{u}, \mathbf{v}, \mathbf{w}$ is defined at time $t = 0$ and so does not change with time. In addition, the features f_1, f_2, n , and hence also h, e, n, θ_p are also constant in time. The state equation of the orbiting object can be expressed as

$$\mathbf{x}(t) = r(t) \{ \cos \theta(t) \mathbf{u} + \sin \theta(t) \mathbf{v} \}, \tag{II.6}$$

in terms of a radial function $r(t)$ and an angular function $\theta(t)$, where

$$\begin{aligned}
r(t) &= (h^2/\mu) / \{ 1 + f_1 \cos \theta(t) + f_2 \sin \theta(t) \} \\
&= (h^2/\mu) / \{ 1 + e \cos(\theta(t) - \theta_p) \}
\end{aligned} \tag{II.7}$$

$$\theta(t) = \theta_p + F_{\text{M-to-T}}(\phi(t) - \phi_p, e), \tag{II.8}$$

$$\begin{aligned}
\phi(t) &= \phi_p + F_{\text{T-to-M}}(\theta(0) - \theta_p, e) + nt \\
&= \phi(0) + nt.
\end{aligned} \tag{II.9}$$

Here $\phi(t)$ denotes the propagated angle on the mean anomaly scale, and $\theta(t)$ denotes the propagated angle on the true anomaly scale, initialized so that $\phi(0) = \theta(0) = 0$. Similarly, $\phi_p = F_{\text{T-to-M}}(\theta_p, e)$ denotes the direction of perigee on the mean anomaly scale where θ_p denotes the corresponding value on the true anomaly scale.

Equation (II.9) shows that on the mean anomaly scale the angular speed n is constant. However, nonlinear mappings, centered at the direction of perigee, are needed to move back and forth between

the mean anomaly and true anomaly scales (equation (II.8)). The Roman letters $T(t)$ and $M(t)$ are used to denote the true and mean anomalies; these angles vanish at perigee. On the other hand, the Greek letters $\theta(t) = T(t) - T(0)$ and $\phi(t) = M(t) - M(0) = nt$ are used to denote the true angular position and its conversion to the mean anomaly scale, initialized so that $\theta(0) = \phi(0) = 0$.

The RTN basis can be contrasted to two related bases:

(a) the *perifocal basis* for which the basis vectors in the $\mathbf{u} - \mathbf{v}$ -plane are given by the direction of perigee and its rotation by 90° . The perifocal convention is unsuitable for a circular orbit (or near-circular orbit) because in this case the direction of perigee is not defined (or is poorly defined), leading to irrelevant “noise” in later calculations.

(b) the *RIC (radial, in-track, cross-track) basis* for which the basis vectors in the $\mathbf{u} - \mathbf{v}$ -plane vary with the time; for each t they point in the radial and tangential directions. Thus the RTN basis is essentially a static version of the RIC basis, after setting the time argument to be the initial time $t = 0$. For our purposes it is more helpful to represent the angular position of the object along its orbit separately from the underlying basis.

III. Coordinate systems

A. Cartesian-ECI coordinates

In *Cartesian earth centered inertial (Cartesian-ECI)* coordinates, the position of an object orbiting the earth is represented with respect to the *standard ECI basis*,

$$\mathbf{u}^{\text{std}} = \begin{bmatrix} 1 \\ 0 \\ 0 \end{bmatrix}, \quad \mathbf{v}^{\text{std}} = \begin{bmatrix} 0 \\ 1 \\ 0 \end{bmatrix}, \quad \mathbf{w}^{\text{std}} = \begin{bmatrix} 0 \\ 0 \\ 1 \end{bmatrix}, \quad (\text{III.10})$$

where \mathbf{w}^{std} points towards celestial north, \mathbf{u}^{std} points towards the vernal direction, and \mathbf{v}^{std} is rotated 90° east about the celestial equator.

Cartesian-ECI coordinates are the simplest coordinates in which to represent the state (i.e. position and velocity) of an orbiting object, $(\mathbf{x}(t), \dot{\mathbf{x}}(t))$, say. In many ways Cartesian-ECI are the easiest coordinates to work with, but they have two main drawbacks. First, the propagation equations are nonlinear, leading to non-Gaussian distributions under propagation (see the next

section). Secondly, the orbital invariants are not obvious in these coordinates.

Hintz [14] provides a concise summary of different coordinate systems for orbital dynamics.

Two of these coordinate systems are described next.

B. Keplerian elements

Keplerian elements form a coordinate system which picks out the orbital invariants explicitly. To define these elements, it is necessary to start with a *reference basis* of \mathbb{R}^3 , specified by three orthonormal vectors $\mathbf{u}^{\text{ref}}, \mathbf{v}^{\text{ref}}, \mathbf{w}^{\text{ref}}$, say, with a positive orientation. Conventionally, the *standard reference basis* from (III.10) is used for the definition of Keplerian elements, but to motivate later sections, a more general choice is allowed in this section.

The first two basis vectors \mathbf{u}^{ref} and \mathbf{v}^{ref} define a *reference plane* (i.e. the “equatorial” plane). In this plane a *preferred reference direction* is given by \mathbf{u}^{ref} and angles in the reference plane can be measured counter-clockwise (i.e. moving from \mathbf{u}^{ref} to \mathbf{v}^{ref}) from the preferred reference direction. Similarly, \mathbf{w}^{ref} can be termed the *normal reference direction*.

The state of the orbiting object determines a second plane, the *orbital plane*. Within the orbital plane, a *preferred orbital direction* can be defined by the direction of perigee, and angles in the orbital plane can be measured counter-clockwise (i.e. in the direction of orbital motion) from the preferred orbital direction.

The intersection between the reference plane and the orbital plane determines a line called the *node line*. This line determines two opposite directions; the RAAN direction is given by the direction for which the projection of the velocity of the orbiting object onto the normal reference direction is positive. Here RAAN stands for Right Ascension of Ascending Node. It is helpful to distinguish between the RAAN *direction*, a unit vector lying on the node line, and the RAAN *angle* Ω , or RAAN for short, specified below.

The Keplerian elements for a state $(\mathbf{x}(t), \dot{\mathbf{x}}(t))$, defined with respect to the specified reference basis, are given as follows:

- $i = \cos^{-1}(\mathbf{w}^T \mathbf{w}^{\text{ref}}) \in [0, \pi]$, the inclination of the orbital plane with respect to the reference plane. Here \mathbf{w} denotes the unit normal vector to the orbital plane.

- $\Omega \in [0, 2\pi)$, the Right Ascension of Ascending Node (RAAN), i.e. the angle in the reference plane from the preferred reference direction to the RAAN direction.
- e , the eccentricity, $0 \leq e < 1$
- $\omega \in [0, 2\pi)$, the argument of perigee, i.e. the angle in the orbital plane from the RAAN direction to the preferred orbital direction.
- a , the major semi-axis, $a > 0$
- $T(t)$, the true anomaly.

Figure 1 illustrates the key directions and angles. Note that the Keplerian elements, except the last one, do not vary with time. Three of these elements, i, Ω, ω , depend on the choice of reference plane; the other three elements, $e, a, T(t)$, do not.

Unfortunately, Keplerian elements are not generally suitable for representing uncertainty by Gaussian distributions. In particular, (a) the RAAN angle Ω becomes undetermined when the orbital plane is either prograde equatorial ($i = 0$) or retrograde equatorial ($i = \pi$), and (b) the argument of perigee (ω) becomes undetermined for a circular orbit ($e = 0$).

C. Equinoctial elements

The problems of Keplerian elements are partly resolved by using a third coordinate system, *equinoctial elements*, denoted E_1, \dots, E_6 and defined as follows (with respect to the same standard reference basis that used above for Keplerian elements):

$$\begin{aligned} E_1 &= 2 \tan(i/2) \cos(\Omega), & E_2 &= 2 \tan(i/2) \sin(\Omega), & E_3(t) &= \Omega + \omega + T(t), \\ E_4 &= e \cos(\Omega + \omega), & E_5 &= e \sin(\Omega + \omega), & E_6 &= a. \end{aligned} \tag{III.11}$$

Some authors replace the major semi-axis a with another quantity depending on the “size” of the ellipse, e.g. the mean motion n [15, 16]. As indicated in the notation, all the coordinates are fixed in time except the third, and $E_1 - E_5$ depend on the reference basis.

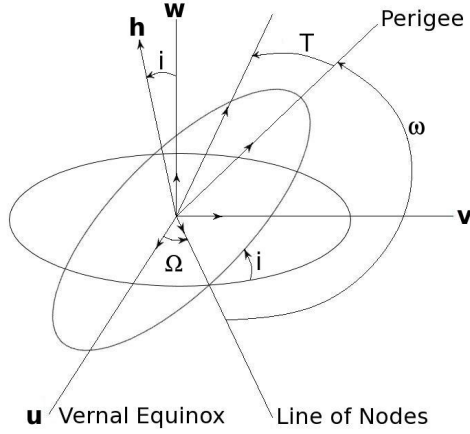


Fig. 1 Orbital dynamics. An orbiting object in Keplerian dynamics. The reference directions $u = u^{\text{ref}}, v = v^{\text{ref}}, w = w^{\text{ref}}$ and the angles ω, Ω, i and $T = T(t)$ are highlighted.

The third coordinate $E_3(t)$ can be termed the *remapped angular position* or *break angle* [17]. If the orbital plane is rotated about the node line onto the reference plane, then $E_3(t)$ represents the angular distance in the reference plane between the preferred reference direction and the image of the position of the orbiting object.

Even though Ω and/or ω may be undetermined in certain circumstances, the equinoctial elements remain well-defined (except for a retrograde equatorial orbit). For example, for a prograde equatorial orbit, E_1 and E_2 equal 0 since $i = 0$, regardless of the fact that Ω is undetermined. Similarly, for a circular orbit E_4 and E_5 equal 0 since $e = 0$. For the remapped angular position E_3 , it is helpful to refer to Figure 1. It can be checked that, except for a retrograde orbit, the sum of angles $\Omega + \omega + T(t)$ remains well-determined even though some of the individual terms become undetermined.

The one situation where equinoctial coordinates break down is for a retrograde orbit ($i = \pi$). The problem can be partly resolved by using one of two possible reference planes, namely the equatorial plane with an upwards or downwards normal, respectively, depending on the orbit to be described (e.g. Cefola [18]), but the solution below using AST coordinates can be applied more automatically and offers more insights.

D. AST coordinates

The final coordinate system to be introduced in this section is the new *Adapted STructral (AST) coordinate system*. The philosophy is somewhat different to the fixed coordinate systems described above. Instead, a *local* or *adapted* coordinate system is used, designed so that uncertainty in the state can generally be represented using Gaussian distributions.

The starting point for AST coordinates is a known approximate value for the state of the orbiting object at time $t = 0$. This value is called the *central state* $(\mathbf{x}^{(c)}(0), \dot{\mathbf{x}}^{(c)}(0))$. The purpose of the central state is to provide a reference basis. Its exact choice does not matter. In general, features related to the central state will be indicated with a superscript $^{(c)}$.

Uncertainty in the initial state vector is represented by a notional point cloud of *deviated states* lying near the central state, with a typical deviated state denoted $(\mathbf{x}(0), \dot{\mathbf{x}}(0))$. In practice the distribution of the deviated states will be modelled by a 6-dimensional Gaussian distribution. The central state will often lie near the middle of the point cloud, but the exact choice does not matter.

Let CRTN stand for the *central RTN basis*, that is, the RTN basis determined from the central state at the initial time $t = 0$. Then AST coordinates, denoted A_1, \dots, A_6 , are defined to be a local version of equinoctial coordinates, that is, the equinoctial coordinates defined with respect to the CRTN basis, with some small adjustments:

$$\begin{aligned} A_1 &= 2 \tan(i/2) \cos(\Omega), & A_2 &= 2 \tan(i/2) \sin(\Omega), & A_3(t) &= \phi(t), \\ A_4 &= e \cos(\theta_p), & A_5 &= e \sin(\theta_p), & A_6 &= n, \end{aligned} \tag{III.12}$$

where the various angles are defined by

$$\theta(t) = \Omega + \omega + T(t) \tag{III.13}$$

$$\theta_p = \Omega + \omega \tag{III.14}$$

$$\phi_p = F_{\text{T-to-M}}(\theta_p, e) \tag{III.15}$$

$$\phi(t) = \phi_p + M(t) \tag{III.16}$$

Note that $A_3(t)$ is the only AST coordinate that varies with time; the others are fixed under Keplerian dynamics.

Conversely, the Keplerian elements with respect the CRTN basis can be defined in terms of AST coordinates by

$$\begin{aligned}
e &= \sqrt{A_4^2 + A_5^2}, \quad \theta_p = \text{atan2}(A_5, A_4), \\
i &= 2 \text{atan} \left(\frac{1}{2} \sqrt{A_1^2 + A_2^2} \right), \quad \Omega = \text{atan2}(A_2, A_1), \\
\omega &= \theta_p - \Omega, \quad a = \mu^{1/3} / A_6^{2/3}, \\
T(t) &= A_3(t) - \theta_p.
\end{aligned} \tag{III.17}$$

Here $T(t)$ is the true anomaly at time t , so that $\theta(t)$ in (III.13) represents the remapped angular direction of the orbital object with respect to the CRTN preferred reference direction. In addition θ_p in (III.14) denotes the direction of perigee with respect to the CRTN preferred reference direction, and ϕ_p in (III.15) denotes the mean anomaly version of this angle. Finally $\phi(t)$ in (III.16) is a mean anomaly version of the information in $\theta(t)$. Note that the initial central angles vanish $\theta^{(c)}(0) = \phi^{(c)}(0) = 0$ but the deviated initial angles $\theta(0) = F_{\text{M-to-T}}(\phi(0), e)$ are small and nonzero.

The AST coordinates differ from equinoctial coordinates in three ways. The most important difference is the choice of reference basis (the CRTN basis for AST coordinates instead of the standard ECI basis for equinoctial coordinates). In particular, the CRTN basis is *adapted* to the distribution of the uncertain state whereas the standard ECI basis is *fixed*. The other two differences are that the angular position of the orbiting object, $A_3(t)$, is represented on the mean anomaly scale rather than the true anomaly scale (and is treated as a number rather than an angle), and that the size of the ellipse, A_6 , is defined by the mean motion n instead of the major semi-axis a . These last two choices are made to linearize the propagation equation (II.9).

A detailed examination of AST coordinates will be given in the next section. For the moment attention is limited to some differences from the standard equinoctial coordinates.

(a) **Retrograde orbits.** Standard equinoctial coordinates break down for a nearly retrograde equatorial orbit (for which the inclination approaches 180°). For AST coordinates the problem does not arise since the inclination of the central state always equals 0° and the inclinations for the deviated states are always close to 0° .

(b) **Linear propagation and winding number.** The system equation (III.16) is a linear func-

tion of $\phi(0)$ and n for fixed time t . Thus if the initial values of $\phi(0)$ and n are Gaussian, the propagated value of $\phi(t)$ remains Gaussian for all future times t .

Further, the use of this representation makes it straightforward to keep track of the *winding number*, that is, how many times the orbiting object has gone around its orbit. More specifically, without any knowledge of the history of the orbiting object, the initial angle $\phi(0)$ only makes sense as an angle; that is $\phi(0)$ and $\phi(0) + 2\pi k$ represent the same angle for any integer k . The initial angle can be turned into a number by restricting it to the interval $[-\pi, \pi)$. Further since deviations from the central angle $\phi^{(c)}(0) = 0$ are assumed small, the values of the deviated angles $\phi(0)$ are always close to 0. Once $\phi(0)$ has been turned into a number, $\phi(t)$ in (III.16) also makes sense as a number, and the integer part of $2\pi(\phi(t) - \phi(0))$ records the whole number of orbits which have occurred by time t .

(c) **Effects of rotation.** Consider first a situation where the CRTN basis equals the standard ECI basis. Hence the central orbital plane is equatorial and the initial central state points towards the standard reference direction, $\mathbf{x}^{(c)}(0) \propto \mathbf{u}^{\text{std}}$. Then the equinoctial and AST coordinates are identical except for small differences in elements 3 and 6. Next rotate the central and deviated orbital planes by 90° to get polar orbits, but keeping the equinoctial reference frame unchanged. The AST coordinates are unchanged. However, since the reference plane for equinoctial coordinates remains equatorial, some of the equinoctial coordinates undergo major changes.

- (i) The third AST coordinate A_3 measures the difference in starting angular position along the orbital path between the deviated and central state. However, for the polar orbit, the third equinoctial coordinate $E_3(0)$ also depends heavily on the RAAN angle Ω . As a result it is messy to interpret the angle $E_3(0)$ as a number near 0 and to develop the winding number interpretation in (b).
- (ii) Suppose that before rotation the first two equinoctial coordinates, describing the deviation from vertical of the normal vector to the orbital plane, are approximately isotropic normal, $N_2(0, \sigma^2 I)$. After rotation to a polar central orbit, the distribution of these coor-

dinates is still approximately isotropic, but the variance becomes inflated (by a factor of 2 for a 90° rotation). The reason is $E_1(0)$ and $E_2(0)$ are defined by a stereographic projection of the sphere, and this projection is known to preserve the shape of a covariance matrix, but not its size [19].

IV. A first order representation for initial AST coordinates

Let

$$R^{(c)} = [\mathbf{u} \ \mathbf{v} \ \mathbf{w}] \quad (\text{IV.18})$$

denote the 3×3 rotation matrix constructed from the central RTN basis using (II.1). Then *standardize* all the deviated states and the central state by defining

$$\mathbf{y}(t) = R^{(c)T} \mathbf{x}(t), \quad \dot{\mathbf{y}}^{(c)}(t) = R^{(c)T} \dot{\mathbf{x}}^{(c)}(t), \quad (\text{IV.19})$$

$$\dot{\mathbf{y}}(t) = R^{(c)T} \dot{\mathbf{x}}(t), \quad \dot{\mathbf{y}}^{(c)}(t) = R^{(c)T} \dot{\mathbf{x}}^{(c)}(t). \quad (\text{IV.20})$$

After standardization, the central state at time $t = 0$ has coordinates

$$\mathbf{y}^{(c)}(0) = \begin{bmatrix} A \\ 0 \\ 0 \end{bmatrix}, \quad \dot{\mathbf{y}}^{(c)}(0) = \begin{bmatrix} B \\ C \\ 0 \end{bmatrix} \quad (\text{IV.21})$$

for parameters $A > 0, B \in \mathbb{R}$, and $C > 0$. A deviated state can then be written in the form

$$\mathbf{y}(0) = \begin{bmatrix} A + \epsilon_1 \\ \epsilon_2 \\ \epsilon_3 \end{bmatrix}, \quad \dot{\mathbf{y}}(0) = \begin{bmatrix} B + \delta_1 \\ C + \delta_2 \\ \delta_3 \end{bmatrix} \quad (\text{IV.22})$$

where ϵ and δ are typically “small”. In this section, a first order Taylor expansion is used to show how the difference in AST coordinates between the deviated and the central state can be approximated

by linear expressions of ϵ and δ ,

$$\mathbf{A} - \mathbf{A}^{(c)} = \mathbf{J} \begin{bmatrix} \epsilon_1 \\ \epsilon_2 \\ \epsilon_3 \\ \delta_1 \\ \delta_2 \\ \delta_3 \end{bmatrix}. \quad (\text{IV.23})$$

where J is the 6×6 Jacobian matrix from Cartesian-ECI to AST coordinates.

The formula for J is derived in Appendix A. The quality of this linear approximation is explored in the next section.

V. Linearity analysis for initial AST coordinates

This section explores numerically the extent to which AST coordinates at the initial time $t = 0$ depend linearly on ϵ and δ . In order to simplify the study to its mathematical essentials, suppose the length and time units are scaled so that the gravitational constant is $\mu = 1$ and the central orbital period is $p = 2\pi$. Then an initial central state can be specified by giving the eccentricity e and the initial true anomaly $T(0)$. The corresponding values of A, B, C are given by

$$A = \frac{h^2}{1 + e \cos T(0)}, \text{ where } h^2 = 1 - e^2,$$

$$C = \frac{h}{A}, \quad B = \frac{e}{AC} \sin T(0).$$

The error variances are most conveniently specified in terms of relative errors. For this study set the position standard error σ to be a specified percentage $P_\sigma\%$ of the geometric mean of the radius at perigee and apogee. Similarly set the velocity standard error τ to be a specified percentage $P_\tau\%$ of the geometric mean of the speed at the perigee and the apogee. In standardized units, these geometric means for position and velocity reduce to h and 1, respectively. More details are given in the Appendix B.

For each component of ϵ and δ , 7 equally spaced values were chosen from -2σ to $+2\sigma$ and -2τ to $+2\tau$, respectively. Then for each AST coordinate and each coordinate of ϵ and δ a plot is

constructed. The plot shows how each AST coordinate varies as the corresponding coordinate of ϵ or δ takes its 7 possible values (with the other components of ϵ and δ fixed at 0). Also superimposed on the plot is a straight line with slope given by the corresponding element of the Jacobian matrix J . Thus a total of 36 plots are generated. If the mapping from ϵ and δ is exactly linear, then the 7 “test values” in each of the 36 plots should lie exactly on a straight line.

Example 1. To judge the quality of the linear approximation for AST coordinates, a challenging set of parameters was chosen, with a high eccentricity, $e = 0.7$, and high relative standard error, $P_\sigma = 2.5\%$, $P_\tau = 20\%$. This eccentricity is at the high end of what is observed in practice. The error rates are far higher than usually found in practice, but are kept small enough to ensure that deviated eccentricity is always less than 1.

Various choices were tried for the initial true anomaly; the choice $T(0) = 45^\circ$ is shown here, but the choice of $T(0)$ has little effect.

Figs. 2-3 show that the linearity approximation is generally very good, even under these extreme conditions. Most of the plots are visually very close to linearity. The worst one is plot (1,6) in Fig. 2 with a squared correlation coefficient of “only” $R^2 = 0.977$; even this plot is acceptably linear for most purposes. Of course the quality of the linear approximation improves with lower standard errors. It also improves with lower eccentricity.

Note that in Figs. 2-3, within each row one ECI coordinate varies over an interval with the other ECI coordinates held fixed. The rows in Fig. 2 correspond to the three ECI position coordinates. The rows in Fig. 3 correspond to the three ECI velocity coordinates.

VI. Propagation under different coordinate systems

Previous sections emphasized the initial behavior of deviated states under different coordinate systems. This section looks at the propagated distributions after a given propagation time t say, under Cartesian-ECI, equinoctial and AST coordinates.

In Cartesian-ECI coordinates all 6 coordinates vary with time. Further, their distribution is subject to the “banana” effect in which uncertainty in the mean motion causes the distribution of the propagated position to become spread out along the orbital path. Equinoctial and AST coordinates

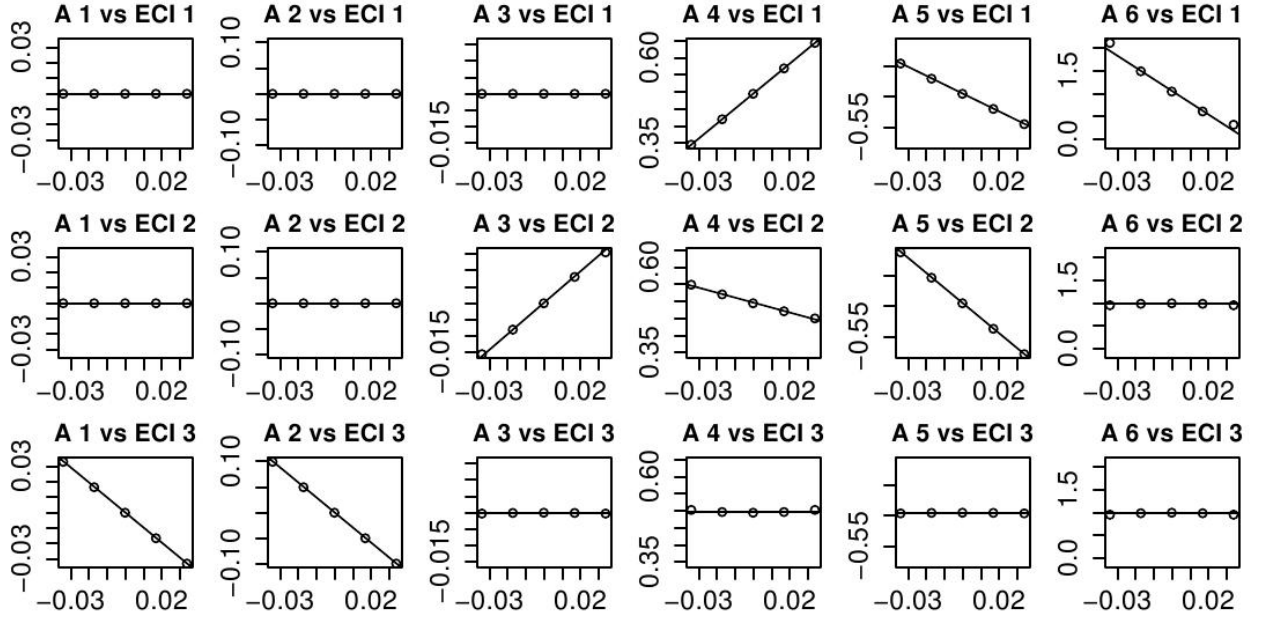


Fig. 2 Example 1. Linearity analysis at time $t = 0$ showing plots of each AST coordinate against the first three ECI coordinates. See also Fig. 3.

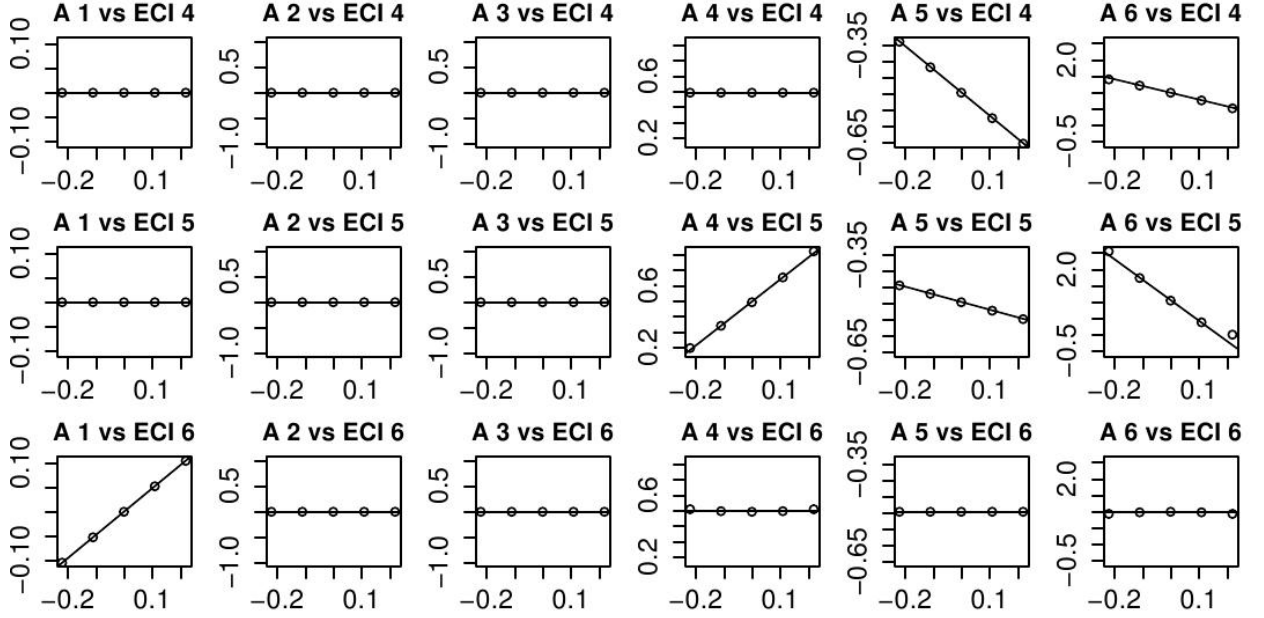


Fig. 3 Example 1. Linearity analysis at time $t = 0$ showing plots of each AST coordinate against the last three ECI coordinates.

are not susceptible to the banana effect, in particular, only the third coordinate ($E_3(t)$ and $A_3(t)$ respectively) varies with time.

The following example illustrates some of the problems with Cartesian-ECI and equinoctial coordinates. Each 6-dimensional propagated distribution is simulated and the resulting point cloud is visualized using a pairs plot. Each pairs plot includes a histogram for each variable and a scatter plot for each pair of variables. The point clouds are based $N = 2000$ simulated initial states. This value of N is more than sufficient to see the patterns of variability in the propagated distributions. Indeed the same patterns can be identified using a much smaller value of N , e.g. $N = 500$.

Example 2. Consider a central orbit with eccentricity $e^{(c)} = 0.7$ (an important parameter) and initial true anomaly $T^{(c)}(0) = 45^\circ$ (a minor parameter). Suppose the relative initial standard deviations are P_σ, P_τ , the same as before. For equinoctial coordinates, the inclination is also an important parameter. If $i^{(c)} = 0$, then equinoctial and AST coordinates are very similar; here let $i^{(c)} = 158^\circ$ to illustrate the problems that can arise for retrograde orbits.

In terms real world situations, if the period is 12 hours (equivalent to $a = 26610$ km), these parameters correspond to a highly eccentric orbit (HEO) with $A = 9078$ km, $B = 2.6$ km/sec and $C = 8.1$ km/sec. Further, $r_a = 45237$ km, $r_p = 7983$ km, $v_a = 1.6$ km/sec and $v_p = 9.21$ km/sec, where r_a, r_p, v_a and v_p indicate radius at the apogee, radius at the perigee, velocity at the apogee and velocity at the perigee respectively.

The state of the object has been propagated for 0.5 central orbital periods. Propagated point clouds have represented as 6-dimensional pairs plot in Cartesian-ECI coordinates (Fig. 4), Equinoctial coordinates with respect to the standard basis (Fig. 5) and AST coordinates (Fig. 6).

From Figs. 4, 5, 6, the following conclusions can be made.

- (a) In **Cartesian-ECI coordinates** (Fig. 4), there is extreme non-Gaussianity. E.g. the scatter plot (2,4) shows severe curvature. Even with much lower standard deviation, there would still often be appreciable curvature in such plots.
- (b) In **Equinoctial coordinates** (Fig. 5), E_1 there is also noticeable non-Gaussianity, e.g. the skewness in E_1 and E_2 . The non-Gaussianity in this example is due to the high inclination of the orbital plane and demonstrates the problems with equinoctial coordinates in this setting.
- (c) In **AST coordinates** (Fig. 6), all the scatter plots are approximately normally distributed.

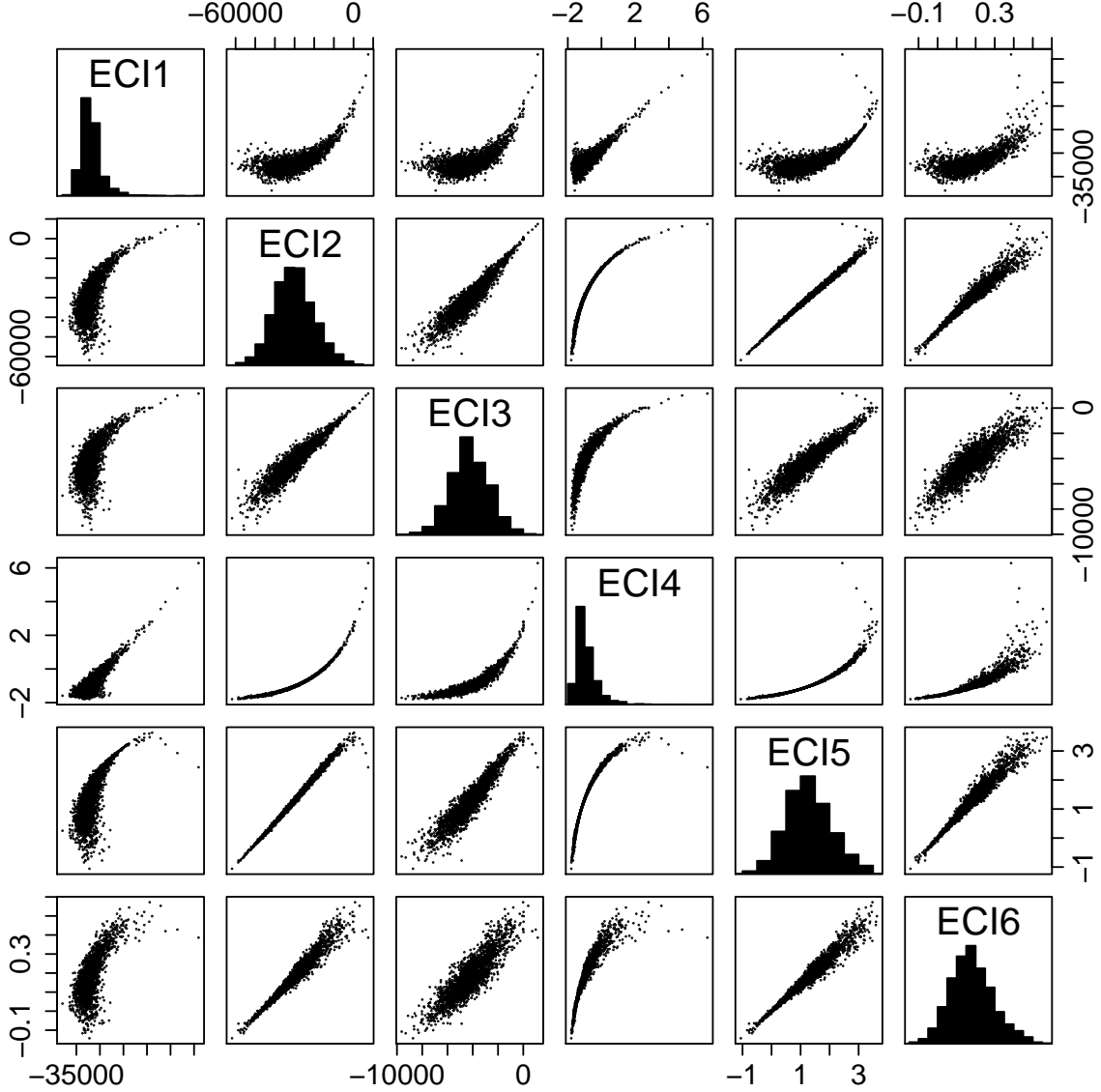


Fig. 4 Example 2, Cartesian-ECI coordinates. Propagated point cloud in Cartesian-ECI coordinates. First three elements represent propagated position vectors (km) and last three elements indicate propagated velocity vectors (km/sec).

Notice the perfect linear relation between elements 3 and 6 ($\phi(t)$ and n) in scatter plot (3,6), which is due to the fact that the uncertainty in $\phi(t)$ is dominated by the variability in n for large t .

It can be shown that non-Gaussianity can be even more severe for Keplerian orbital elements [20].

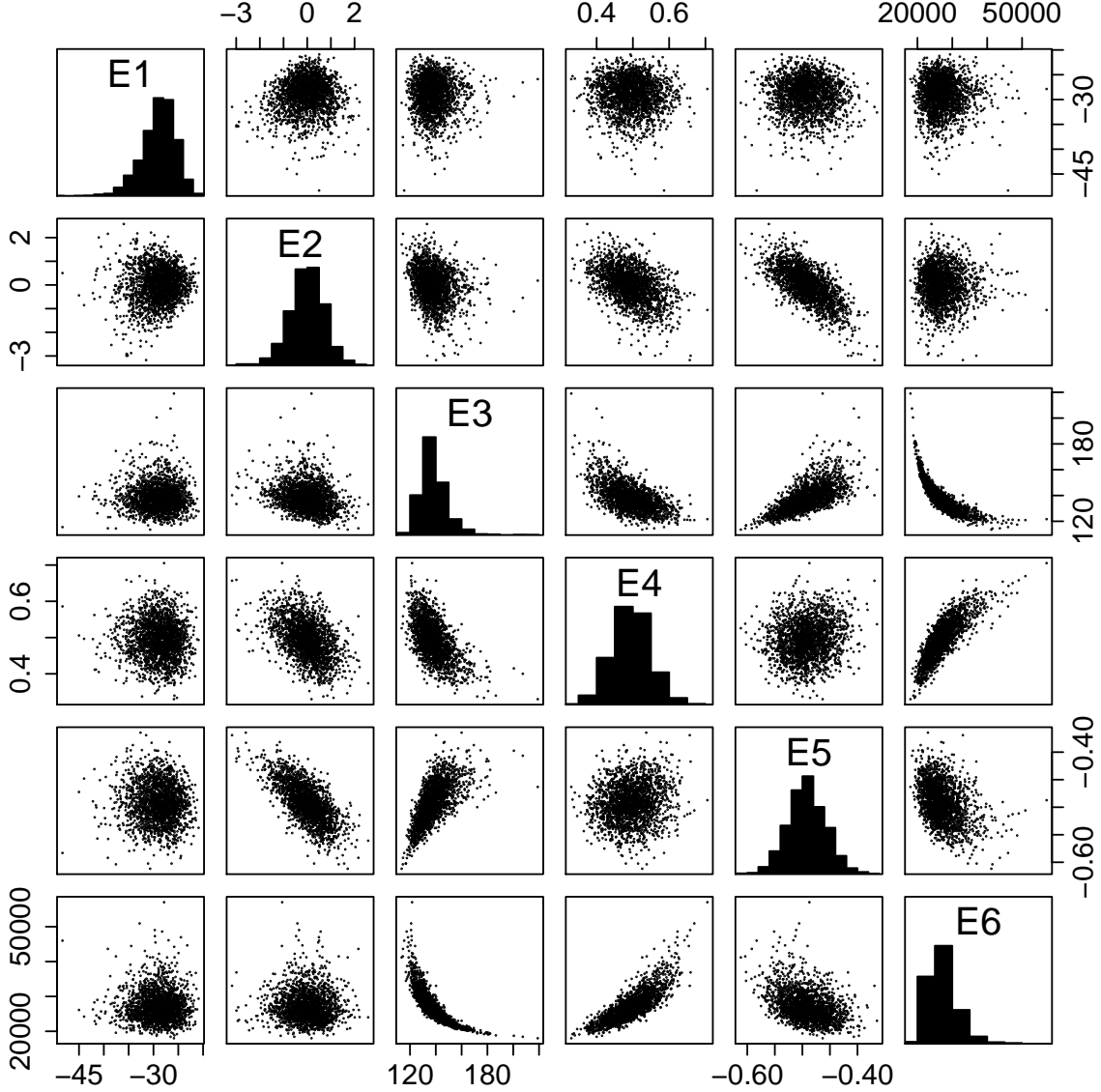


Fig. 5 Example 2, equinoctial coordinates. Propagated point cloud in equinoctial coordinates.

VII. Statistical analysis for propagated distributions

An important criterion for a “good” coordinate system is that a point cloud at the initial (and propagated) times should look approximately Gaussian, given an initial Gaussian distribution in Cartesian-ECI coordinates. In the previous section Gaussianity was judged visually. In this section these judgments are backed up with formal statistical tests. Two suitable test statistics were developed by Mardia [21] to assess skewness and kurtosis, respectively and have been implemented

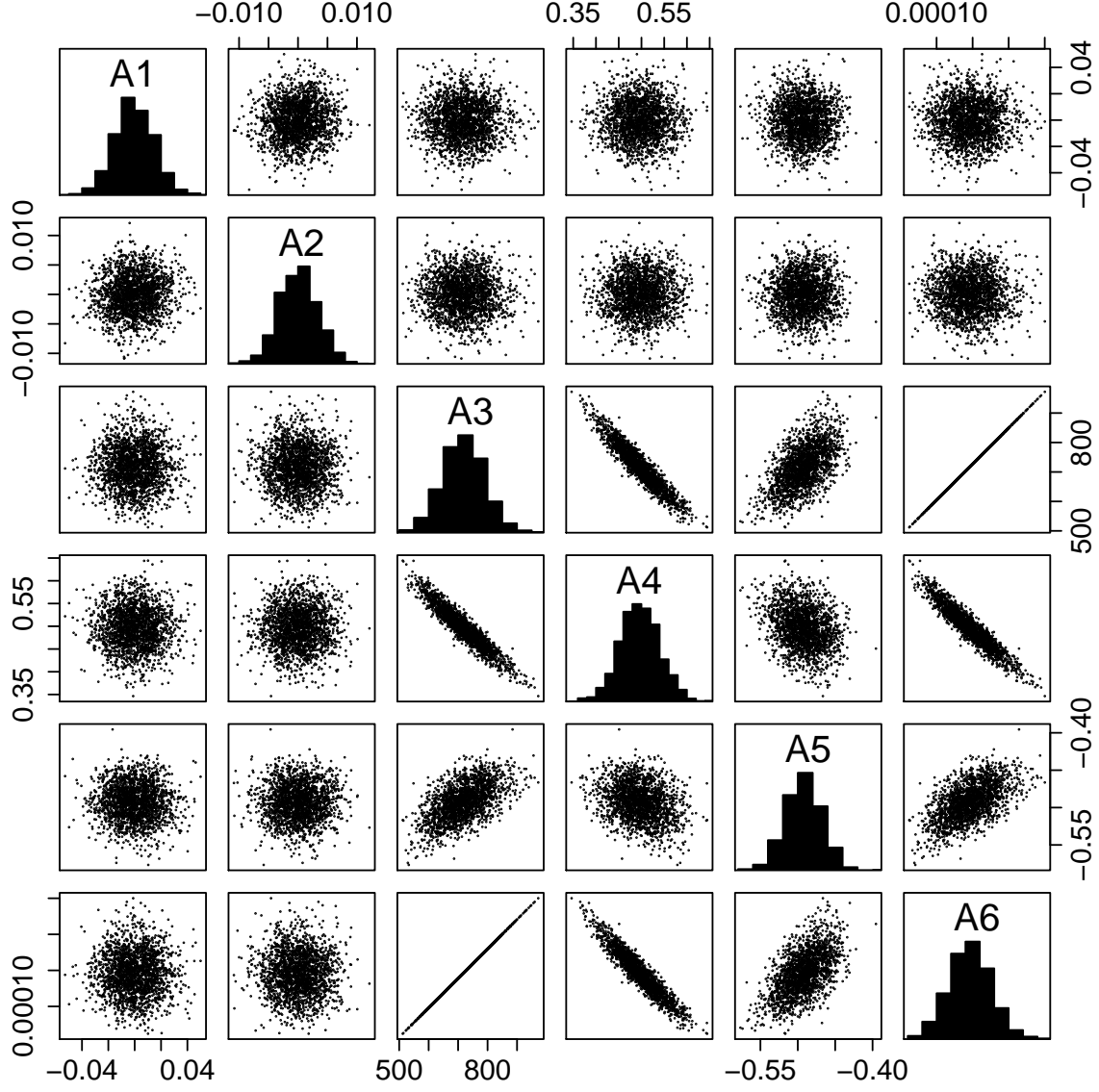


Fig. 6 Example 2, AST coordinates. Propagated point cloud in AST coordinates. All the histograms and scatter plots are approximately normal.

in R [22].

For simplicity attention is restricted to testing the full 6-dimensional point cloud for Gaussianity under each of our coordinate systems. The results of each test can be summarized by a p-value. If Gaussianity holds, the p-value will be uniformly distributed between 0 and 1. However, if normality fails, then the p-value will tend to be close to 0. To carry out a formal statistical test, a small

threshold α is chosen (e.g. $\alpha = 0.05$) and if the p-value is below the threshold, then the hypothesis of Gaussianity is rejected. For each pairs plot, two p-values have been computed, for skewness and kurtosis, respectively. The p-values for the *Example 2* are summarized in Table 1. For both the Cartesian-ECI and the equinoctial coordinate system p-values are very small. These results reinforce our visual impression.

Caution- The power of a statistical test depends on the sample size (here the number of simulated points in the point cloud). If the underlying distribution is even slightly non-normal, then for a large enough sample size, the hypothesis of normality will be eventually rejected. Here a sample size of $N = 2000$ has been used, which is adequate to confirm the approximate normality in Fig. 6, and to strongly reject normality in most of the plots in Figs. 4 and 5. In Table 1, for the Cartesian-ECI and equinoctial coordinate systems very small p-values ($< 1e-20$) are effectively 0 and indicate the distribution is extremely non-Gaussian.

Table 1 Normality test results. Here $p_{\text{skewness}}, p_{\text{kurtosis}}$ represent p-values for skewness and kurtosis respectively.

Coordinate system	p_{skewness}	p_{kurtosis}
Cartesian-ECI (Fig. 4)	$< 1e-20$	$< 1e-20$
Equinoctial (Fig. 5)	$< 1e-20$	$< 1e-20$
AST coordinates (Fig. 6)	0.27	0.4

VIII. Filtering using the AST coordinate system

The main purpose behind the development of AST coordinates is to facilitate the tracking of space objects. Assume that each observation takes the form of an angles-only position measurement (a unit vector \mathbf{z}_{obs}), which can be represented using “latitude” $\psi_{\text{obs}} \in [-\pi/2, \pi/2]$ and “longitude” $\theta_{\text{obs}} \in [-\pi, \pi)$, defined with respect to the CRTN frame. In general, a latitude ψ and longitude θ determine unit vector \mathbf{z} by

$$z_1 = \cos \psi \cos \theta, \quad z_2 = \cos \psi \sin \theta, \quad z_3 = \sin \psi.$$

Longitude is measured on true anomaly scale (if there were no errors the the observation would satisfy the identity $\theta_{\text{obs}} = \theta_p + T(t)$ would hold where t is the propagation time), whereas AST

element 3 ($A_3(t) = \phi(t)$) is computed on the mean anomaly scale. The transformation from mean anomaly to true anomaly can be extremely non-linear under high ellipticity. Fig. 7 shows the relation when $e = 0.7$.

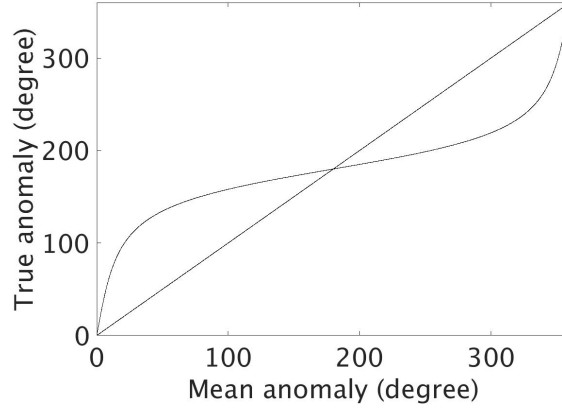


Fig. 7 Mean anomaly to true anomaly. The horizontal axis represents the mean anomaly and the vertical axis represents the true anomaly, both in degrees between 0° and 360° .

Next consider the update stage of the Kalman filter. In particular, it requires a 6-dimensional variance matrix for the propagated state $\mathbf{A}(t)$, and a 2-dimensional measurement variance matrix for $(\theta_{obs}, \psi_{obs})$. Of these the most interesting components are the propagated variance of $A_3(t)$ and the measurement variance of the longitude θ_{obs} . If the ellipticity is high, then a nonlinear version of the Kalman filter is needed. Common choices are the unscented and extended Kalman filters (UKF and EKF) [23–26].

However, if in addition the propagation time is large, then the propagated variance of $A_3(t)$ can be much larger than the measurement variance of θ_{obs} . In such a situation the UKF and EKF can perform very poorly. The reason is that they deal with the nonlinearity by taking a first order Taylor expansion (discrete or exact) centered at the propagated mean of $A_3(t)$, whereas it is much better to center the first order Taylor expansion at or near the measurement value $F_{T\text{-to-M}}(\theta_{obs}, e)$, where e is the eccentricity for the mean propagated state.

These issues are discussed in more detail in a companion paper [27], which makes 4 suggestions: (a and b) newly developed observation-centered Kalman filters, (c and d) iterated Kalman filters such as the IEKF [28] and IUKF. This paper uses IUKF for update steps. Note that one advantage

of the OCEKF and OCUKF over the IEKF and the IUKF is that they do not require iteration. However, an advantage of the IEKF and the IUKF over the OCEKF and the OCUKF is that they are more widely applicable. In situations where measurement error is not small, the posterior moments from the IEKF and IUKF can be closer to the true posterior moments. Of course, a particle filter can be used to solve the tracking problem, but it is not needed here. Simple and very effective solutions are available using first order approximations.

From equations (III.12)–(III.16) and from Chapter 4 in [10] the spherical coordinates $(\theta(t), \psi(t))$ can be written in terms of Keplerian elements as

$$\begin{aligned}\theta(t) &= \Omega + \omega + T(t), \\ \psi(t) &= \sin^{-1} \{ \sin(L_1) \sin(L_2(t)) \},\end{aligned}$$

where $L_1 = 2 \tan^{-1} i$ and $L_2(t) = \omega + T(t)$. In turn, the Keplerian elements can be written in terms of the AST coordinates using equation (III.17).

The AST-IUKF steps are briefly summarized below.

Given

- a. The central state in Cartesian-ECI coordinates at time $t_0 = 0$;
- b. The covariance matrix associated with the central state in Cartesian-ECI coordinate system;
- c. Sequence of angles-only measurements at times $t_1 < t_2 < \dots$;

Computation

- 1) Find the CRTN frame at time t_0 ;
- 2) Compute the initial mean state and its covariance matrix in AST coordinates at time t_0 , set $\nu = 0$;
- 3) Propagate the mean and variance of the AST state distribution from time t_ν to time $t_{\nu+1}$;
- 4) Transform the angles-only measurements at time $t_{\nu+1}$ to CRTN coordinates;
- 5) Update the AST state mean and variance using the IUKF at $t_{\nu+1}$;
- 6) Set $\nu \rightarrow \nu + 1$ and repeat stages 3), 4) and 5) for each observation;

Algorithm 1: AST-IUKF stages

Note: There is no need to update the CRTN frame at each iteration.

A. Examples (filtering)

This section analyses two examples. The first example (Example 3) illustrates the one-step update; the purpose is to show the limitations of the EKF and the UKF when the orbital eccentricity is high, the propagated variance is large and the observation variance is small.

The second example (Example 4) deals a more realistic tracking problem, using the IUKF algorithm along with the AST coordinate system to track a space object.

Example 3, One-step update. Assume an uncertain orbiting object with central ellipticity $e^{(c)} = 0.7$ and with initial relative standard errors $P_\sigma = 2.5\%$, $P_\tau = 20\%$ in Cartesian-ECI coordinates, the same as in Examples 1 and 2. For simplicity here assume the central inclination vanishes, $i^{(c)} = 0^\circ$ and the central angle of perigee is $\theta_p^{(c)} = 0^\circ$. Recall from (II.9) that the propagated variance of $A_3(t)$ increases linearly with t . Choose the propagation time t_1 large enough that the standard deviation of $A_3(t)$ equals $\sigma^* = 25^\circ$. Also suppose that the propagated mean of $A_3(t)$ is $\mu^* = 260^\circ$. This value is chosen to highlight the nonlinearity of $F_{T\text{-to-M}}$.

Consider an angles-only observation with longitude $\theta_{obs} = 225.5^\circ$ and latitude $\psi_{obs} = 0^\circ$ in the CRTN frame of reference, with measurement standard deviation $5.5\text{e-}04^\circ$ (2 arc-seconds) for both. Note that the longitude of the observation, after transformation to the mean anomaly scale, takes the value

$$\phi_{obs} = F_{T\text{-to-M}}(225.5^\circ, 0.7) = 310^\circ,$$

which is located at the 2.5% upper tail of the propagated distribution for $A_3(t_1)$ since $\phi_{obs} = \mu^* + 2\sigma^* = 260^\circ + 2 \times 25^\circ = 310^\circ$. Such cases are mildly unusual but not unlikely.

The propagated distribution for $A_3(t_1)$ forms the prior in the Bayesian update. Since the measurement standard deviation is very small (2 arc-seconds), the posterior mean for the $A_3(t_1)$ is concentrated very close to 310° . The nonlinearity of the function $F_{M\text{-to-T}}$ between 260° and 310° leads to striking differences between the various filters. The results are summarized in Table 2. For the “Exact” entry in this table, the posterior mean and variance have been computed using a particle filter [29, 30] with one million particles. Table 2 shows that that EKF and UKF give

Table 2 Posterior means and standard deviations for $A_3(t_1)$ in Example 3, computed using various filters.

Moment	UKF	IUKF	EKF	IEKF	OCUKF	OCEKF	“Exact”
mean (A_3)	327.1°	310°	329.8°	310°	310°	310°	310°
s.d (A_3)	4.1e-04°	3.2e-02°	5e-04°	3.1e-02°	3.2e-02°	3.3e-02°	3.2e-02°

terrible approximations to the posterior distribution but the IUKF, IEKF, OCEKF and OCUKF all give excellent approximations.

The “Exact” columns gives the correct answer showing that the posterior is highly concentrated about 310°. The IUKF, IEKF, OCUKF and OCEKF filters are all similar to one another and the exact answer. However, the UKF and EKF are terrible filters. Their 95% probability intervals are incompatible with the exact 95% probability interval.

Example 4, Tracking. The purpose of this example is to describe effectiveness of the AST-IUKF algorithm for a sequence of measurements. Consider the same setup used in Example 2, and consider a sequence of 200 hourly angles-only observations, with standard deviations 0.1° in the in-track and cross-track directions. The results are summarized using Figs. 8 and 9. In order to judge the performance of the AST-IUKF, two sets of plots have been generated and analyzed. A brief description is given below.

(a) **Log scaled variance plots.** Intuitively the AST posterior variances for $A_1(t_\nu)$ to $A_5(t_\nu)$ are expected to decrease at rate $O(1/t_\nu)$, and the posterior variance for $A_6(t_\nu)$ to decrease at rate $O(1/t_\nu^2)$. To visualize this behavior, Fig. 8 shows plots of $\log_e\{A_j(t_\nu)t_\nu\}$, $j = 1, \dots, 5$ and $\log_e\{A_6(t_\nu)t_\nu^2\}$ vs. t_ν . The log transform is used so that a few initial outliers do not distort the plot. As expected, except for a few initial values, each plot is approximately a horizontal straight line.

(b) **Log scaled absolute difference plots.** Similarly, Fig. 9 shows plots of $\log_e\{D_j(t_\nu)t_\nu^{1/2}\}$, $j = 1, \dots, 5$ and $\log_e\{A_6(t_\nu)t_\nu\}$ vs. t_ν , where $D_j(t_\nu)$ denotes the absolute difference between the true AST value and the updated AST mean at time t_ν , for $j = 1, \dots, 6$. As expected, up to sampling error all the plots are approximately horizontal straight lines.

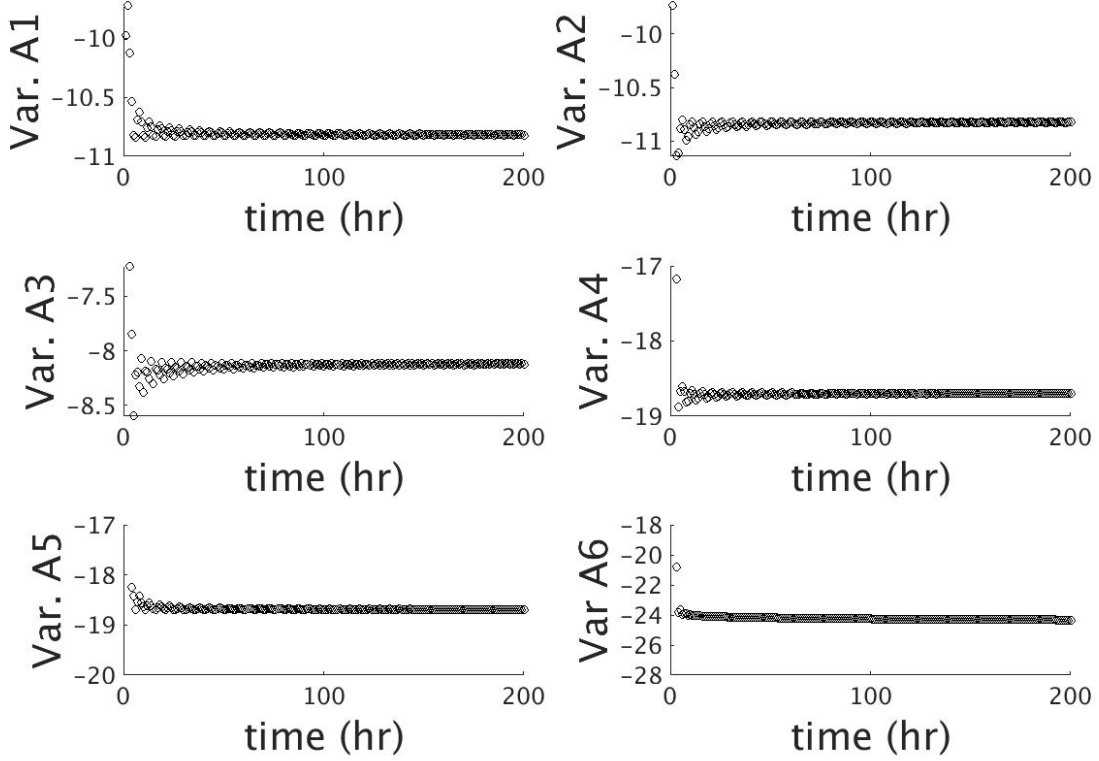


Fig. 8 Example 4, Log scaled variance plots. The log scaled updated AST variances vs. time for A1-A6.

IX. Conclusion

To summarize, this paper has investigated two types of nonlinearity. The first type is the nonlinearity in the propagation equations in Cartesian-ECI coordinates. A first-order Taylor expansion was used to represent the AST deviations at time $t = 0$ as approximately linear functions of the ECI deviations. This expansion helps to explain why AST coordinates are generally typically approximately Gaussian whenever the initial conditions are. These conclusions are reinforced by the linearity plots in Section V, even under extreme initial uncertainties.

The second type of nonlinearity arises from the difference between the true anomaly and mean anomaly in the tracking problem. If the orbital eccentricity is high then standard tracking algorithms such as EKF or UKF sometimes fail to approximate the posterior mean and variance accurately. However, the iterated Kalman filters such as the IUKF, IEKF and the newly developed OCEKF

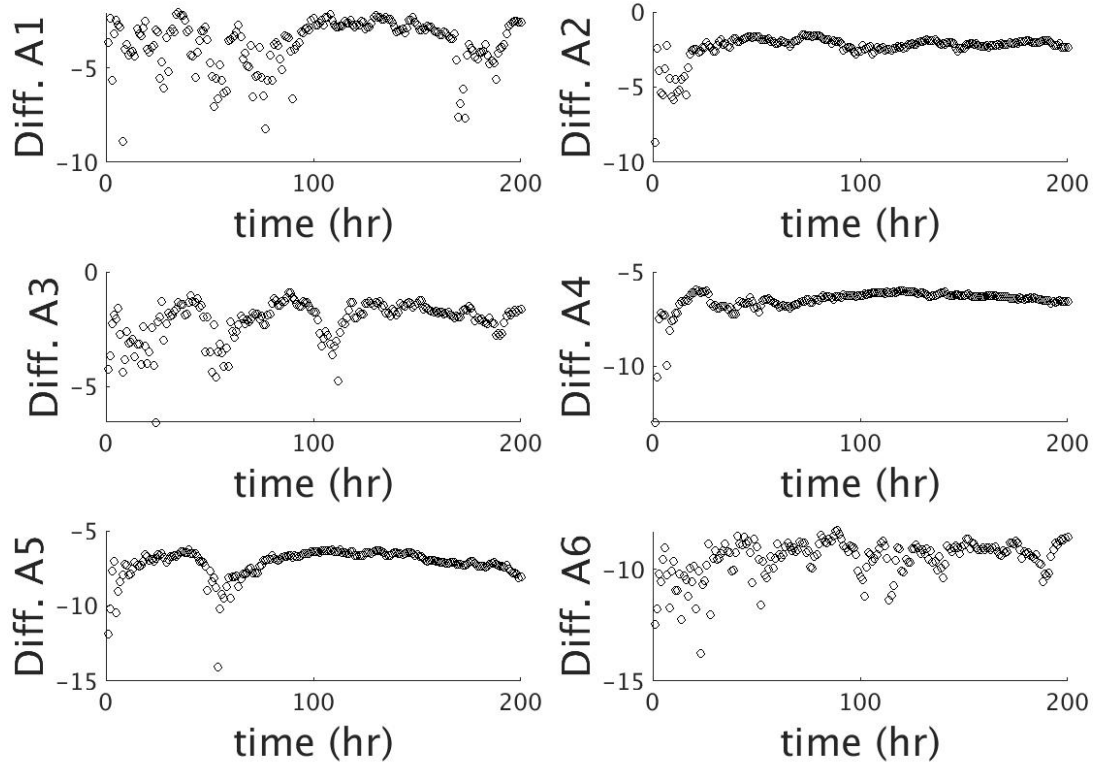


Fig. 9 Example 4, Log scaled absolute difference plots. The log scaled absolute differences between the true AST values and the updated AST means vs. time for A1-A6.

and OCUKF work well in this situation.

Appendix

A. The Jacobian for the mapping from Cartesian-ECI to AST coordinates.

The purposos of this appendix is to show that the Jacobian \mathbf{J} in (IV.23) between Cartesian-ECI coordinates and AST coordinates at time $t = 0$ takes the form

$$\mathbf{J} = \begin{array}{cccccc} \epsilon_1 & \epsilon_2 & \epsilon_3 & \delta_1 & \delta_2 & \delta_3 \\ \left[\begin{array}{cccccc} 0 & 0 & -B/AC & 0 & 0 & 1/C \\ 0 & 0 & -1/A & 0 & 0 & 0 \\ 0 & D/A & 0 & 0 & 0 & 0 \\ C^2/\mu - 1/A & -BC/\mu & 0 & 0 & 2AC/\mu & 0 \\ -BC/\mu & B^2/\mu - 1/A & 0 & -AC/\mu & -AB/\mu & 0 \\ P_1C + P_2Q_1 & -P_1B + P_2Q_2 & 0 & P_1A + 2P_2A^2BC^2 & P_2Q_3 & 0 \end{array} \right] & \begin{array}{l} A1 \\ A2 \\ A3 \\ A4 \\ A5 \\ A6 \end{array} \end{array}$$

where

$$\begin{aligned} D &= \frac{(1 - e^{(c)^2})^{3/2}}{(1 + e^{(c)} \cos T^{(c)})^2} \\ P_1 &= -\frac{3}{2} \frac{n^{(c)}}{h^{(c)^2}} 2AC \\ P_2 &= -\frac{3}{2} \frac{n^{(c)}}{h^{(c)^2}} \frac{a^{(c)}}{\mu} \\ Q_1 &= \{(2C^2 - \frac{2\mu}{A})(AC^2 - \mu) + 2AB^2C^2\} \\ Q_2 &= \{-2BC(AC^2 - \mu) - 2AB^3C + BC\mu\} \\ Q_3 &= \{4AC(AC^2 - \mu) + 2A^2B^2C\}. \end{aligned}$$

Here is the derivation, with all expansions taken to first order in ϵ and δ . The superscript $^{(c)}$ denotes the value of a parameter for the central state. Recall that in y -coordinates (IV.21)–(IV.22), the CRTN basis is the same as the standard basis.

Expansion for $A_1(0)$ and $A_2(0)$. The angular momentum vector can be expressed as

$$\begin{aligned} \mathbf{h} &= \mathbf{x} \times \dot{\mathbf{x}} \\ &= \begin{bmatrix} \epsilon_2 \delta_3 - \epsilon_3 (C + \delta_2) \\ \epsilon_3 (B + \delta_1) - (A + \epsilon_1) \delta_3 \\ (A + \epsilon_1)(C + \delta_2) - \epsilon_2 (B + \delta_1) \end{bmatrix} \approx \begin{bmatrix} -\epsilon_3 C \\ \epsilon_3 B - A \delta_3 \\ AC + A \delta_2 + C \epsilon_1 - \epsilon_2 B \end{bmatrix} \end{aligned}$$

with squared norm

$$h^2 \approx A^2 C^2 + 2AC(A\delta_2 + C\epsilon_1 - B\epsilon_2).$$

That is,

$$h^2 \approx h^{(c)2} + \Delta_{h^2},$$

where $h^{(c)} = AC$ and

$$\Delta_{h^2} = 2AC(A\delta_2 + C\epsilon_1 - B\epsilon_2).$$

The first two components of $\mathbf{w} = \mathbf{h}/h$ simplify to

$$w_1 \approx -\epsilon_3 C, \quad w_2 \approx \epsilon_3 B - A \delta_3.$$

In terms of Keplerian elements,

$$w_1 = \sin i \sin \Omega \approx i \sin \Omega, \quad w_2 = -\sin i \cos \Omega \approx -i \cos \Omega$$

since the inclination angle i is small. Further, the first two AST coordinates are given by

$$2 \tan(i/2) \sin(\Omega) \approx i \sin(\Omega) \approx w_1, \quad 2 \tan(i/2) \cos(\Omega) \approx i \cos(\Omega) \approx -w_2,$$

thus confirming the first two rows of J .

Expansion for $A_4(0)$ and $A_5(0)$. After a bit of calculation, the expression for the eccentricity vector \mathbf{e} simplifies to

$$\mathbf{e} \approx \frac{1}{\mu} \begin{bmatrix} AC^2 + 2\delta_2 AC + \epsilon_1 C^2 - \epsilon_2 BC - \mu - \mu \epsilon_1 / A \\ -ABC - \delta_1 AC - \epsilon_1 BC - \delta_2 AB + \epsilon_2 B^2 - \mu \epsilon_2 / A \\ -\delta_3 AB - \epsilon_3 B^2 - \epsilon_3 C^2 - \mu \epsilon_3 / A \end{bmatrix},$$

and since $\mathbf{e} = f_1 \mathbf{u}^{(e)} + f_2 \mathbf{v}^{(e)}$ from (II.4),

$$\begin{aligned} f_1 &\approx \frac{1}{\mu} (AC^2 + 2\delta_2 AC + \epsilon_1 C^2 - \epsilon_2 BC - \mu - \mu\epsilon_1/A), \\ f_2 &\approx \frac{1}{\mu} (-ABC - \delta_1 AC - \epsilon_1 BC - \delta_2 AB + \epsilon_2 B^2 - \mu\epsilon_2/A). \end{aligned}$$

The first order error terms determine rows 4 and 5 of J .

Expansion for $A_6(0)$. The squared norm of \mathbf{e} becomes

$$\begin{aligned} e^2 &\approx \frac{1}{\mu^2} \{ (AC^2 - \mu)^2 + 2(2\delta_2 AC + \epsilon_1 C^2 - \epsilon_2 BC - \mu\epsilon_1/A)(AC^2 - \mu) \\ &\quad + (ABC)^2 2(\delta_1 AC + \epsilon_1 BC + \delta_2 AB - \epsilon_2 B^2 + \mu\epsilon_2/A)(ABC) \} \\ &= \{e^{(c)}\}^2 + \Delta_{e^2} \end{aligned}$$

where

$$\begin{aligned} \{e^{(c)}\}^2 &= \frac{1}{\mu^2} \{ (AC^2 - \mu)^2 + (ABC)^2 \}, \\ \Delta_{e^2} &= \frac{1}{\mu^2} \{ 2(2\delta_2 AC + \epsilon_1 C^2 - \epsilon_2 BC - \mu\epsilon_1/A)(AC^2 - \mu) \\ &\quad + 2(\delta_1 AC + \epsilon_1 BC + \delta_2 AB - \epsilon_2 B^2 + \mu\epsilon_2/A)(ABC) \}. \end{aligned}$$

Then a takes the form

$$\begin{aligned} a &= \frac{h^2}{\mu} \frac{1}{1 - e^2} \\ &\approx \frac{h^{(c)^2}}{\mu} \frac{1}{1 - e^{(c)^2}} \left(1 + \frac{\Delta_h^2}{h^{(c)^2}} + \frac{\Delta_e^2}{1 - e^{(c)^2}} \right) \\ &= a^{(c)} + \Delta_a, \end{aligned}$$

where

$$\begin{aligned} a^{(c)} &= \frac{h^{(c)^2}}{\mu} \frac{1}{1 - e^{(c)^2}} \\ &= - \frac{A^2 C^2}{A^2 B^2 C^2 / \mu + A^2 C^4 / \mu - 2AC^2} \\ &= \frac{A\mu}{2\mu - AB^2 - AC^2}. \end{aligned}$$

and

$$\Delta_a = a^{(c)} \left(\frac{\Delta_h^2}{h^{(c)^2}} + \frac{\Delta_e^2}{1 - e^{(c)^2}} \right).$$

The mean motion n is the same as the sixth AST coordinate A_6 and can be expressed as

$$\begin{aligned} n &= (\mu/a^3)^{1/2} = \{\mu/(a^{(c)} + \Delta_a)^3\}^{1/2} \\ &= (\mu/a^{(c)3})^{1/2} \{1 - \frac{3}{2} \Delta_a/a^{(c)}\} \\ &= n^{(c)} + \Delta_n \end{aligned}$$

where $n^{(c)} = \{\mu/a^{(c)3}\}^{1/2}$ and

$$\begin{aligned} \Delta_n &= -\frac{3}{2} n^{(c)} \Delta_a/a^{(c)} \\ &= -\frac{3}{2} (n^{(c)}/a^{(c)}) \{\Delta_{h^2}/h^{(c)2} + \Delta_{e^2}/(1 - e^{(c)2})\} \\ &= -\frac{3}{2} \frac{n^{(c)}}{h^{(c)2}} (\Delta_{h^2} + \mu a^{(c)} \Delta_{e^2}), \end{aligned}$$

since $1/(1 - e^{(c)2}) = \mu a^{(c)}/h^{(c)2}$. Simplifying this expression yields the sixth row of J .

Expansion for $A_3(0)$. For this section, write the first order representation of the deviated basis at time $t = 0$ in more concise notation as

$$\begin{bmatrix} \mathbf{u} & \mathbf{v} & \mathbf{w} \end{bmatrix} = \begin{bmatrix} 1 & -a & -b \\ a & 1 & -c \\ b & c & 1 \end{bmatrix},$$

where $a = \epsilon_2/A$, $b = \epsilon_2/A$, $c = \delta_3/C - \epsilon_3 B/AC$. The RANN direction Ω can be represented as a unit vector \mathbf{k} , say, proportional to the vector cross product

$$\mathbf{w} \times \mathbf{w}^{(c)} = \begin{bmatrix} -b \\ -c \\ 1 \end{bmatrix} \times \begin{bmatrix} 0 \\ 0 \\ 1 \end{bmatrix} = \begin{bmatrix} -c \\ b \\ 0 \end{bmatrix}.$$

After rescaling to a unit vector, $\mathbf{k} = \begin{bmatrix} -c' \\ b' \\ 0 \end{bmatrix}$, where $[b', c'] = [b, c]/\sqrt{b^2 + c^2}$.

Rotate the initial deviated point $\mathbf{y}(0)$ to the equatorial plane by the rotation G , say, which keeps the node line fixed, and set $\mathbf{y}^* = G\mathbf{y}$. Then the angle $\theta(0)$ in (III.13) can be described as the angle in the equatorial plane from $[1 \ 0 \ 0]^T$ to \mathbf{y}^* .

Write G to first order in the form

$$G = I + Q = \begin{bmatrix} 1 & q_{12} & q_{13} \\ -q_{12} & 1 & q_{23} \\ -q_{13} & -q_{23} & 1 \end{bmatrix},$$

where Q is skew symmetric. The condition $G\mathbf{k} = \mathbf{k}$ implies that $q_{12} = 0$ and $q_{13}c - q_{23}b = 0$.

The condition $R\mathbf{w} = [0 \ 0 \ 1]^T$ implies, after ignoring terms higher than first order, that $q_{13} = b$, $q_{23} = c$.

Hence to first order

$$\mathbf{y}^* = R\mathbf{y} = \begin{bmatrix} 1 \\ a \\ 0 \end{bmatrix},$$

and so the angle from $\mathbf{u}^{(c)}$ is given by

$$\text{atan2}(a, 1) = a = \epsilon_2/A. \quad (\text{IX.24})$$

The final step is to transform from the true anomaly scale to the mean anomaly scale. The value of $\theta(0)$ is related to the true anomaly by $\theta(0) = \theta_p + T(0)$ and

$$\begin{aligned} \phi(0) &= F_{\text{T-to-M}}(\theta_p, e) + F_{\text{T-to-M}}(T(0), e) \\ &= T_{\text{T-to-M}}(\theta(0) - T(0), e) - F_{\text{T-to-M}}(-T(0), e) \\ &\approx \theta(0)F'_{\text{T-to-M}}(-T(0), e) = \theta F'_{\text{T-to-M}}(T(0), e) \\ &\approx \theta(0)F'_{\text{T-to-M}}(T^{(c)}(0), e^{(c)}). \end{aligned}$$

The derivative is well-known (e.g. [10]),

$$(d/dT)F_{\text{T-to-M}}(T, e) = \frac{(1 - e^2)^{3/2}}{(1 + e \cos T)^2} = \frac{(1 - e^2)^{3/2}}{(1 + f_1)^2}. \quad (\text{IX.25})$$

It does not matter to first order whether the deviated or central value is used since f_1 and e are close to $f_1^{(c)}$ and $e^{(c)}$. Combining (IX.24) and (IX.25) leads to the third line of J .

B. Standardized units

Section V refers to certain identities for orbital elements when standardized units are used for length and time, so that the gravitational constant is $\mu = 1$ and the central orbital period is $p = 2\pi$.

From (II.2)–(II.3) it follows that $a = 1$ and $h^2 = (1 - e^2)$. Hence from [10] the standard formulas for the radius at apogee and perigee, and the velocity at apogee and perigee, simplify to

$$\begin{aligned} r_a &= \frac{h^2}{\mu} \frac{1}{1 + e \cos \pi} = \frac{h^2}{\mu} \frac{1}{1 - e} = 1 + e, \\ r_p &= \frac{h^2}{\mu} \frac{1}{1 + e \cos 0} = \frac{h^2}{\mu} \frac{1}{1 + e} = 1 - e, \\ v_a &= \sqrt{\frac{(1 - e)}{(1 + e)} \frac{\mu}{a}} = \sqrt{\frac{(1 - e)}{(1 + e)}}, \\ v_p &= \sqrt{\frac{(1 + e)}{(1 - e)} \frac{\mu}{a}} = \sqrt{\frac{(1 + e)}{(1 - e)}}. \end{aligned}$$

Therefore, geometric means become $\sqrt{r_a r_p} = \sqrt{1 - e^2}$, $\sqrt{v_a v_p} = 1$.

Acknowledgment

This material is based upon work supported by the Air Force Office of Scientific Research, Air Force Materiel Command, USAF under Award No. FA9550-19-1-7000.

References

- [1] G. Sibley, G. Sukhatme, L. Matthies, “The Iterated Sigma Point Kalman Filter with Applications to Long Range Stereo”, Robotics: Science and Systems II conference, August 2006.
- [2] J.L.Junkins, M.R. Akella, K.T. Alfriend, “Non-Gaussian error propagation in orbital mechanics”, Journal of the Astronautical Sciences, Vol. 44, pp. 541–563, 1996.
- [3] I. Park, D. J. Scheeres, “Hybrid method for uncertainty propagation of orbital motion”, Journal of Guidance, Control, and Dynamics, Vol. 41, No. 1, pp. 240–254, 2018.
- [4] R. S. Park, D. J. Scheeres, “Nonlinear mapping of gaussian statistics: theory and applications to spacecraft trajectory design”, Journal of Guidance, Control, and Dynamics, Vol. 29, No. 6, pp. 1367–1375, November-December 2006.
- [5] K. Fujimoto, D. J. Scheeres, “Analytical nonlinear propagation of uncertainty in the two body problem”, Journal of Guidance, Control, and Dynamics, Vol. 35, No. 2, pp. 497–509, 2012.
- [6] V. Vittaldev, R. P. Russell, R. Linares, “Spacecraft uncertainty propagation using Gaussian mixture models and polynomial chaos expansions”, Journal of Guidance, Control, and Dynamics, Vol. 39, No. 12, pp. 2615–2626, 2016.
- [7] R. Bhusal, K. Subbarao, “Generalized polynomial chaos expansion approach for uncertainty quantification in small satellite orbital debris problems”, The Journal of the Astronautical Sciences, Springer US, Vol. 0021-9142, pp. 1–29, 2019.
- [8] X. Fenfena, C. Shishia, X. Ying, “Dynamic system uncertainty propagation using polynomial chaos”, Chinese Journal of Aeronautics, Vol. 27, No. 5, pp. 1156–1170, October 2014.
- [9] J. T. Horwood, A. B. Poore, “Non linear mapping of uncertainties in celestial mechanics, Gauss-von-Mises distribution for improved uncertainty realism in space situational awareness”, SIAM/ASA J. Uncertainty Quantification, Vol. 2, pp. 276–304, 2014.
- [10] H. Curtis, “Orbital mechanics for engineering students”, Elsevier Aerospace Engineering Series, ISBN-10: 008102133X, ISBN-13: 978-0081021330, 2006.
- [11] W. E. Wiesel, “Spaceflight Dynamics”, CreateSpace Independent Publishing Platform, 3rd edition, ISBN-13: 978-1452879598, 2010.

- [12] C. A. Kluever, “Space Flight Dynamics”, Aerospace Series, Wiley-Blackwell, 2nd edition, ISBN-13: 978-1119157823, 2018.
- [13] R. Fitzpatrick, “An Introduction to Celestial Mechanics”, Cambridge University Press, ISBN-13: 978-1107023819, 2012.
- [14] G. R. Hintz, “Survey of orbit element sets”, Journal of Guidance, Control, and Dynamics, Vol. 31, No. 3, pp. 785–790, 2008.
- [15] J. H. Jo, I. K. Park, N. Choe, M. Choi, “The comparison of the classical Keplerian orbit elements, non-singular orbital elements (equinoctial elements), and the Cartesian state variables in Lagrange planetary equations with J_2 perturbation: Part I”, JASS, Vol. 28, No. 1, pp. 37–54, 2011.
- [16] M. J. H. Walker, B. Ireland, J. Owens, “A set modified equinoctial orbit elements”, Celestial mechanics, Vol. 36, No. 4, pp. 409–419, August 1985.
- [17] A. E. Roy, “Orbital Motion”, Routledge, 4 edition, ISBN-13: 978-0750310154, 2004.
- [18] P. CEFOLA, “Equinoctial orbit elements - application to artificial satellite orbits”, AIAA/AAS Astrodynamics Conference, Palo Alto, CA, U.S.A., September 1972.
- [19] F. W. Sohon, “The Stereographic Projection”, Literary Licensing, LLC, 2013, ISBN-1258625385, 9781258625382.
- [20] J. T. Kent, S. Bhattacharjee, I. I. Hussein, M. K. Jah, “Nonlinear filtering using directional statistics for the orbital tracking problem with perturbation effects”, Proceedings of the 28th AAS/AIAA Space Flight Mechanics Meeting, 2018.
- [21] K. V. Mardia, “Measures of multivariate skewness and kurtosis with applications”, Biometrika, Vol. 57, pp. 519–530, 1970.
- [22] S. Korkmaz, D. Goksuluk, G. Zararsiz, “MVN: An R package for assessing multivariate normality”, The R Journal, Vol. 6, pp. 151–162, 2014.
- [23] S. J. Julier, J. K. Uhlmann, “Unscented filtering and nonlinear estimation”, IEEE Proc., Vol. 92, pp. 401–422, 2004.
- [24] F. Gustafsson, G. Hendeby, “Some Relations Between Extended and Unscented Kalman Filters”, IEEE Transactions on Signal Processing, Vol. 60, No. 2, pp. 545–555, 2012.
- [25] E.A. Wan, R. V. D. Merwe, “The unscented Kalman filter for nonlinear estimation”, Proc. of the IEEE 2000 Adaptive Systems for Signal Processing, Communications, and Control Symposium, October 2000.
- [26] J. J. LaViola, “A comparison of unscented and extended Kalman filtering for estimating quaternion motion”, Proc. American Control Conf., pp. 2435–2440, 4-6 June 2003.
- [27] J. T. Kent, S. Bhattacharjee, W. R. Faber, I. I. Hussein, “observation-centered Kalman filter”,

arXiv:1907.13501.

- [28] J. Havlík, O. Straka, “Performance evaluation of iterated extended Kalman filter with variable step-length”, *Journal of Physics: Conference Series*, IOP Publishing, Vol. 659, pp. 12–22, 2015.
- [29] F. Gustafsson, F. Gunnarsson, N. Bergman, U. Forssell, J. Jansson, R. Karlsson, P.-J. Nordlund, “Particle filters for positioning navigation and tracking”, *IEEE Trans. Signal Processing*, Vol. 50, No. 2, pp. 425–437, February 2002.
- [30] J. McCabe, K. DeMars, “Particle Filter Methods for Space Object Tracking”, *AIAA/AAS Astrodynamics Specialist Conference*, 2014.